

## Step Motion, Patterns, and Kinetic Instabilities on Crystal Surfaces

Daniel Kandel<sup>1</sup> and John D. Weeks<sup>1,2</sup>

<sup>1</sup>*Institute for Physical Science and Technology, University of Maryland, College Park, Maryland 20742*

<sup>2</sup>*Department of Chemistry, University of Maryland, College Park, Maryland 20742*

(Received 12 November 1993)

We study a mesoscopic kinetic model for step flow on crystal surfaces in the presence of impurities. The evolution of the system of steps in the small line tension limit leads to the formation of complex highly connected step patterns. We identify repeating features in the patterns and calculate them analytically by analyzing a simplified mean-field-like model. For the same model we also calculate analytically the coarsening with time of the typical length scale associated with the patterns. All the analytical results are in excellent quantitative agreement with numerical simulations.

PACS numbers: 61.50.Cj, 68.55.Jk

The behavior of atomic steps on surfaces of crystals is of major importance for crystal growth and evaporation processes [1-3]. For example, vicinal surfaces have been used successfully as substrates for the fabrication of nanostructures (e.g., quantum wires) with the molecular beam epitaxy technique [2]. Stepped surfaces are particularly useful for these purposes in the *step flow* regime [4], where crystal growth proceeds predominantly by the motion of fairly straight and uniformly spaced steps. However, in some cases the uniform step system becomes kinetically unstable, leading to the appearance of straight bunches of steps, steps with fingerlike shapes, and even complex highly connected networks of steps (as we demonstrate below).

One possible mechanism [5] leading to an instability was suggested by Frank [6]. He argued physically that the adsorption on the surface of impurities possessing the following two properties could lead to step bunching. (i) An impurity impedes the motion of a step segment immediately behind it. (ii) After the step segment has moved past or covered an impurity, its effect on subsequent steps can be ignored.

This idea has been further developed by other researchers [7-10], but only in the limit where the steps remain straight throughout the entire bunching process. Here we examine the implications of Frank's picture using more general two dimensional (2D) models that allow fluctuations along the step edges.

Our starting point is a semimicroscopic or mesoscopic 2D model for step flow in the presence of impurities [11], which we analyzed previously in the large line tension limit [10] (where steps remain basically straight during the entire bunching process). Consider  $N$  steps on a square lattice (with periodic boundary conditions in both directions), where each step is composed of  $L$  coarse-grained segments that reside on the links of the lattice. We associate a "line tension" energy favoring straight steps with each configuration of segments:  $E = \gamma \sum_{n,y} [x_n(y+1) - x_n(y)]^2$ , where  $x_n(y)$  is the position of the  $y$ th segment of step  $n$ , and  $\gamma$  is the effective line tension.

In the absence of impurities, a simplified treatment of the diffusion of main component atoms [10] leads to the following rules for step motion: (1) Select a step segment at random, say segment  $y$  of step  $n$ . (2) Attempt to move it backwards with probability  $p_b = (1 - A)/2$ , or forward with probability  $p_f = p_b + A\{1 - \exp[-W_n(y)/l_d]\}$ . Here  $W_n(y) \equiv x_{n+1}(y) - x_n(y)$  is the local terrace width,  $l_d$  is the main component diffusion length, and  $A$  is a monotonically increasing function of the flux of main component atoms, which vanishes when the flux is equal to the equilibrium flux. (3) Always reject the attempted move if it leads to terraces of width smaller than 1. (This corresponds to overhanging steps.) If this no-overhang condition is not violated, reject the move with probability  $1 - \exp(-\beta\Delta E)$  if it raises the line tension energy by an amount  $\Delta E$ , and accept it otherwise. Here  $\beta$  is the inverse temperature. At equilibrium, with  $A = 0$ , these rules reproduce the usual Monte Carlo kinetics of steps where fluctuations (whose magnitude is controlled by a line tension) generate an entropic repulsive interaction.

Now consider the adsorption of impurities which incorporate properties (i) and (ii) of Frank's model [6,10]. Such impurities arrive at random vacant sites of the lattice (multiple occupancy is prohibited). When attempting to move a step segment forward past an impurity, the acceptance probability of the move is reduced by a factor  $0 < 1 - S < 1$  compared to the probability in the absence of an impurity [rule (3) above]. If the move is accepted, the impurity no longer affects step motion. The microscopic parameter  $S$  is associated with the strength of impurities. If  $S \approx 0$  the impurities are weak, whereas  $S \approx 1$  is the strong impurity limit.

We simulate the model in the following way. Starting with uniformly spaced straight steps and a surface free of impurities, we alternately perform sweeps of impurity deposition and step flow. In an impurity deposition sweep we pick at random  $F_i NLW^0$  sites, where  $F_i$  is the flux of impurities and  $W^0$  is the initial terrace width. Impurities are deposited in all the selected *vacant* sites. Each step flow sweep consists of  $NL$  attempts to move step segments chosen at random. The attempts are done

according to rules (1)–(3) above, taking into account the effects of impurities on step motion as well.

Figure 1(a) is a snapshot of a system of  $N = 30$  steps of  $L = 1000$  segments each, after 25 000 time steps. The values of the parameters we used are  $K \equiv \beta\gamma = 0.1$ ,  $S = 0.65$ ,  $F_i = 0.005$ ,  $l_d = 10$ , and  $A = 0.9$ . The resulting step pattern is very complex and highly connected. However, several simple repeated features can be easily noticed: (a) Although the steps are not straight, one can still identify fairly long straight portions of steps that have bunched together. (b) There exist points at which a bunch splits into two smaller bunches; we call these points *vertices*. Several vertices are marked on the pattern of Fig. 1(a) by dashed lines. Note that typically the bunch of steps is straight near the vertex and forms a well defined angle, say  $\alpha$ , with the  $y$  axis (the step orientation in the initial configuration). After splitting at the vertex, one of the emerging bunches continues in the direction of the original bunch, while the other makes a turn and goes in the  $-\alpha$  direction. (c) The pattern divides the surface into cells. Many of them have the typical shape marked by dash-dotted lines in Fig. 1(a). At the perimeter of each cell we find vertices, and straight as well as curved

portions of step bunches.

As time passes, small cells shrink in size, while big cells expand, leading to coarsening of all the structures of the step pattern. However, the features we emphasized above do not change during this evolution. Even the value of the angle  $\alpha$  remains constant.

Our aim now is to understand quantitatively the features of the patterns, and the growth of the typical length scale with time. In order to perform analytical calculations, we consider a simpler 2D mean-field-like model for the evolution of the stepped surface. This simply adds a line tension term to the 1D models for step bunching previously hypothesized by other researchers [7–9], and also implicitly assumed by Frank [6]. According to this model, the local terrace widths obey the following differential equations:

$$\frac{\partial W_n(y)}{\partial t} = f[W_{n+1}(y)] - f[W_n(y)] + \bar{\gamma} \frac{\partial^2 W_n(y)}{\partial y^2}, \quad (1)$$

where the continuous variable  $y$  replaces the discrete coordinate of the mesoscopic model, and the index  $n$  increases in the direction of step flow.

The first two terms on the right hand side (r.h.s.) of (1) induce step flow and account for the effect of impurities. We showed in Ref. [10] that in the large line tension limit Eq. (1) yields an accurate mean field description of the mesoscopic model presented above. We calculated the velocity function  $f$  analytically, and our results were in excellent quantitative agreement with numerical simulations of the mesoscopic model. The resulting function  $f(W)$  has the following properties: it vanishes for vanishing terrace width, and increases with  $W$  for small values of  $W$ . It has a maximum at  $W = W^m$ , and for  $W > W^m$  it decreases exponentially to the value  $f(\infty) > 0$ .

The last term on the r.h.s. of (1) permits fluctuations along a step controlled by a line tension. The parameter  $\bar{\gamma}$  is an increasing function of the effective line tension  $\gamma$ . Thus, if  $\bar{\gamma} \rightarrow \infty$  the steps are completely straight, and (1) reduces to the 1D models considered in Refs. [7–9].

We solved (1) numerically with  $\bar{\gamma} = 0.1$ , after adding a noise term to the r.h.s., using the velocity function  $f$  that results from the mean field theory of Ref. [10]. In Fig. 1(b) we show a snapshot of the system. The pattern is clearly very similar to that of Fig. 1(a) with the same features: the typical angle  $\alpha$ , the vertices, and the typical cell shape.

Even this simplified model is not easy to solve analytically. To yield quantitative predictions we make several additional assumptions. First, the presence of repeating features in step patterns that slowly coarsen with time is most naturally explained by assuming the system is locally close to a set of *weakly unstable* steady state solutions of Eq. (1).

Next, we note that the characteristic features appear fairly early in the evolution of the system. At that stage, each bunch of steps contains only a few steps. We there-

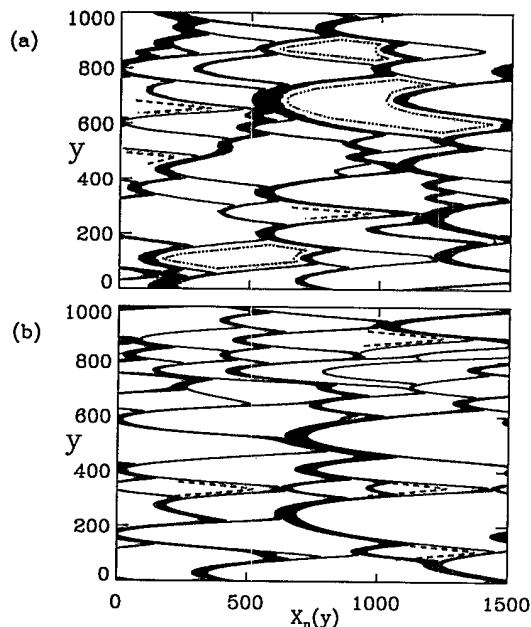


FIG. 1. (a) A snapshot of a step system after 25 000 time steps of the mesoscopic kinetic model. The simulation parameters are  $K = 0.1$ ,  $S = 0.65$ ,  $F_i = 0.005$ ,  $l_d = 10$ , and  $A = 0.9$ . Steps move from left to right and are marked by solid lines. Heavy solid lines correspond to step bunches. Dashed lines mark vertices, while typical cell shapes are shown as dash-dotted lines. (b) A snapshot of a step system evolving according to model (1) with noise. The function  $f$  came out of a mean field calculation [10] with the parameters of (a). We used  $\bar{\gamma} = 0.1$ . The vertex structure of the infinite period steady state is shown by dashed lines.

fore conclude that these features are due to effects that are local in the step index,  $n$ . Hence, it is sufficient to calculate steady states which are periodic in  $n$ ; we do not expect the periodicity to alter the predictions significantly. It is also convenient to consider such states, because the evolution equation (1) preserves periodicities in the step index.

Consistent with these assumptions, we now characterize all the steady states of (1), which are of period two in the step index  $n$ . (We expect higher periods to yield similar results.) We will also perform a linear stability analysis of the resulting solutions, to confirm that they are indeed weakly unstable. This analysis will lead to a prediction of the coarsening of the patterns.

The period two restriction takes the form  $W_n(y, t) + W_{n+1}(y, t) = 2\bar{W}$ , with  $\bar{W}$  independent of  $y$  and  $t$ . Using this relation for  $W_{n+1}$  in (1), we obtain an evolution equation for  $W_n$  that is independent of the width of other terraces. Equating  $\partial W_n(y, t)/\partial t$  to zero, we get the following steady state equation:

$$\bar{\gamma} \frac{d^2 W_n^s}{dy^2} = -\frac{dV}{dW_n^s}, \quad (2)$$

where  $W_n^s(y)$  is the steady state solution, and the "potential"  $V$  has the form

$$V(W_n^s) \equiv \int^{W_n^s} [f(2\bar{W} - W) - f(W)] dW. \quad (3)$$

Equation (2) obviously has the form of Newton's second law for a particle moving in the potential  $V$  in one dimension.  $W_n^s$  is the analog of the position of the particle,  $\bar{\gamma}$  is the mass, and  $y$  is analogous to time.

Since  $f$  is undefined for negative terrace widths, we look for solutions of (2) and (3) where the motion of the particle is bounded in the interval  $0 \leq W_n^s \leq 2\bar{W}$ . The particle's trajectory depends on the shape of the potential  $V$ , which in turn depends on the velocity function  $f$  and on the value of the average terrace width  $\bar{W}$ .

The most interesting case arises when  $\bar{W} > W^m$  (a discussion of all the solutions will be presented elsewhere [12]). Then  $V$  is symmetric about its minimum at  $W_n^s = \bar{W}$ , and has two maxima at  $W_n^s = \bar{W} \pm \Delta$ , where  $\Delta < \bar{W}$  depends on the function  $f$ . There is a continuous family of solutions of Eq. (2), which are periodic in "time" (the  $y$  coordinate). They are all bounded in the interval  $\bar{W} - \Delta \leq W_n^s \leq \bar{W} + \Delta$ , and can be characterized by the integral of the motion of Eq. (2) that corresponds to the "energy" of the Newtonian particle:

$$\mathcal{E} = \frac{1}{2} \bar{\gamma} \left( \frac{dW_n^s}{dy} \right)^2 + V[W_n^s(y)]. \quad (4)$$

$\mathcal{E}$  is independent of  $y$ , and can take any value in the interval  $[V(\bar{W}), V(\bar{W} + \Delta)]$ . The extremal points of the solution associated with a particular value of  $\mathcal{E}$  are  $W^\pm(\mathcal{E})$ , such that  $V(W^\pm) = \mathcal{E}$ ,  $W^+ > W^-$ , and  $W^+ + W^- =$

$2\bar{W}$ .  $W_n^s$  visits  $W^\pm$  periodically, and the period  $l(\mathcal{E})$  is given as

$$l(\mathcal{E}) = 4\sqrt{\frac{\bar{\gamma}}{2}} \int_{\bar{W}}^{W^+} \frac{dW}{\sqrt{\mathcal{E} - V(W)}}. \quad (5)$$

We argue that these solutions explain the features of the patterns mentioned above and the coarsening of the typical length scale. For example, each periodic solution takes the value  $W_n^s = \bar{W}$  twice every period. Each occurrence of this value of the terrace width corresponds to a vertex where a pair of steps splits in two. The vertex is localized in a very small region of space (see Fig. 1) because when  $W_n^s = \bar{W}$ , the "kinetic energy" of the Newtonian particle is maximal and it stays there for a very short "time."

To obtain the angle  $\alpha$ , note that the period  $l$  diverges [see Eq. (5)] when  $\mathcal{E}$  approaches its maximal value  $V(\bar{W} + \Delta)$ . This solution corresponds to an infinite length scale steady state with a single vertex. Far from the vertex, the solution approaches a straight line that defines the angle  $\alpha$ . In other steady states, with  $\mathcal{E}$  smaller but close to  $V(\bar{W} + \Delta)$ ,  $x_n(y)$  is straight over fairly long intervals, and the angle associated with the straight portions is very close to the one obtained from the infinite period solution. This property of the long period solutions is general and holds for any velocity function  $f$  with the properties defined above.

For certain forms of the function  $f$ , we can express steady states in closed analytic form [12]. However, for quantitative comparisons with simulations, we must numerically analyze the solutions of (2) using the particular form of  $f$  corresponding to the pattern of interest, say Fig. 1(b), for example. Figure 2 presents such a solution with a finite period in the  $y$  direction. Note the similarity between the steady state cell structure and the structure of cells in Fig. 1. The existence of vertices and of the well defined angle is also apparent in Fig. 2. We can also compute the infinite period steady state in the same way. The vertex structure and the angle  $\alpha$  of that steady state are drawn as dashed lines in Fig. 1(b) near vertices of the

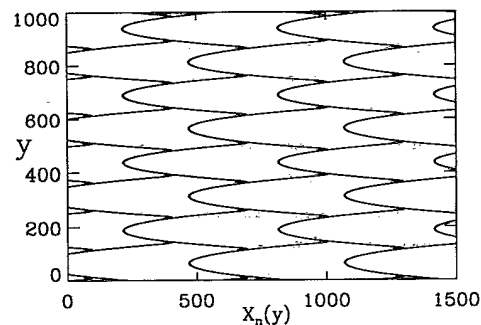


FIG. 2. A finite period steady state calculated for the function  $f$  of Fig. 1(b) and  $\bar{\gamma} = 0.1$ .

pattern. The agreement between theory and simulations is certainly impressive.

Finally, we show that the steady states we calculated are weakly unstable. To that end, we linearize Eq. (1) (with the period two restriction) to first order in the quantity  $\delta W_n(y, t) \equiv W_n(y, t) - W_n^s(y)$ . Since the resulting equation is linear, we can separate the variables  $y$  and  $t$  by defining  $\delta W_n(y, t) \equiv g(y)h(t)$ . The solution for  $h$  is  $h(t) \sim \exp(\omega t)$ , with  $\omega$  being the eigenvalue of the Schrödinger-like equation

$$-\gamma \frac{d^2 g}{dy^2} - \frac{d^2 V}{d(W_n^s)^2} g = -\omega g \quad (6)$$

for the wave function  $g$  of a quantum mechanical particle moving in the periodic potential  $-d^2 V/d(W_n^s)^2$ . The energy eigenvalue is  $-\omega$ . It is easy to see that  $g = dW_n^s/dy$  is a solution of (6) with eigenvalue  $\omega = 0$ . Thus for every steady state,  $W_n^s$ , there is a marginal perturbation.

To find out whether these states are actually unstable or only marginal, we have to calculate the most unstable perturbation. This eigenfunction corresponds to the maximal value of  $\omega$  and to the ground state of the Schrödinger equation (6). For the infinite period [ $\mathcal{E} = V(W^+)$ ] steady state solution,  $dW_n^s/dy$  is the ground state because it has no nodes. Hence the single vertex steady state is marginal. The other periodic steady states turn out to be unstable [12], but those states for which  $\mathcal{E}$  is close to the maximal value are only weakly unstable as we anticipated above.

We now expand expression (5) for the period, around  $\mathcal{E} = V(W^+)$ . We can also expand  $\omega^{\max}$ , the maximal value of  $\omega$ , around  $\mathcal{E} = V(W^+)$ , and use the two expansions to obtain an expression for  $l$  in terms of  $\omega^{\max}$ . To leading order we get  $l \sim 1/\sqrt{\omega^{\max}}$ . Assuming that the relevant time scale for coarsening is  $1/\omega^{\max}$  we deduce that  $l \sim t^{1/2}$ . Note that we predict a much faster coarsening process than the one we predicted [10] for the large line tension limit ( $l \sim \ln t$ ). Our numerical simulations of the mesoscopic model are consistent [12] with the average cell size growing as  $t^{1/2}$ , but more extensive simulations are needed in order to provide an accurate quantitative test.

In summary, the ansatz that our step system is always locally close to a weakly unstable steady state leads to analytical predictions of step patterns and their coarsening. These predictions are in excellent quantitative agreement with simulations of the mesoscopic step flow

model. Moreover, they can be directly compared with experimental results, using essentially a single fitting parameter (the impurity strength  $S$ ). Other parameters can be obtained independently from experiments. For example, the line tension parameter can be estimated from an analysis of step fluctuations [13]. We therefore hope that our well defined predictions for this system will lead to experimental searches for the phenomena discussed in this work.

We thank N.C. Bartelt, M.E. Fisher, E.D. Williams, and Y.-N. Yang for stimulating discussions. This work was supported in part by the National Science Foundation under Grant No. NSF-DMR-91-03031.

- [1] H. Yasunaga and A. Natori, Surf. Sci. Rep. 15, 205 (1992), and references therein.
- [2] P. M. Petroff, A. C. Gossard, and W. Wiegmann, Appl. Phys. Lett. 45, 620 (1984); M. S. Miller, H. Weman, C. E. Pryor, M. Krishnamarthy, P. M. Petroff, H. Kroemer, and J. L. Merz, Phys. Rev. Lett. 68, 3464 (1992).
- [3] S. Iwanari and K. Takayanagi, J. Cryst. Growth 119, 229 (1992).
- [4] W. K. Burton, N. Cabrera, and F. C. Frank, Philos. Trans. R. Soc. London, Ser. A 243, 299 (1951).
- [5] For other mechanisms see, e.g., R. L. Schwoebel, J. Appl. Phys. 40, 614 (1969); G. S. Bales and A. Zangwill, Phys. Rev. B 41, 5500 (1990).
- [6] F. C. Frank, in *Growth and Perfection of Crystals*, edited by R. Doremus, B. Roberts, and D. Turnbull (Wiley, New York, 1958), p. 411; see also N. Cabrera and D. A. Vermilyea, *ibid.*, p. 393.
- [7] P. Bennema and G. H. Gilmer, in *Crystal Growth: an Introduction*, edited by P. Hartman (North-Holland, Amsterdam, 1973), p. 263.
- [8] J. P. v. d. Eerden and H. Muller-Krumbhaar, Phys. Rev. Lett. 57, 2431 (1986); Phys. Scr. 40, 337 (1989).
- [9] D. Kandel and J. D. Weeks, Phys. Rev. Lett. 69, 3758 (1992); Physica (Amsterdam) 66D, 78 (1993).
- [10] D. Kandel and J. D. Weeks, Phys. Rev. B 49, 5554 (1994).
- [11] We argued in Ref. [10] that the impurities need not come from an external source. Generalized impurities can result from local perturbation of the surface structure caused by the kinetic process itself. This makes the model applicable to much more general experimental conditions.
- [12] D. Kandel and J. D. Weeks (unpublished).
- [13] N. C. Bartelt, J. L. Goldberg, T. L. Einstein, E. D. Williams, J. C. Heyraud, and J. J. Métois, Phys. Rev. B 48, 15 453 (1993).